ISSN 1674-1056
http://cpb.iphy.ac.cn
http://iopscience.iop.org/cpb
中国物理 B
Chinese Physics
中国物理
Chinese Physics B

Phase transition and near-zero thermal expansion of Zr

Jun-Ping Wang(王俊平), Qing-Dong Chen(陈庆东), Sai-Lei Li(李赛磊), Yan-Jun Ji(纪延俊), Wen-Ying Mu(穆文英), Wei-Wei Feng(冯伟伟), Gao-Jie Zeng(曾高杰), You-Wen Liu(刘友文), Er-Jun Liang(梁二军)
Citation: Chin. Phys. B . 2018, 27(6): 066501. **doi:** 10.1088/1674-1056/27/6/066501

Journal homepage: http://cpb.iphy.ac.cn; http://iopscience.iop.org/cpb

What follows is a list of articles you may be interested in

Negative thermal expansion and photoluminescence in solid solution $(HfSc)_{0.83}W_{2.25}P_{0.83}O_{12\delta}$

Yuan Liang(梁源), Yong-Guang Cheng(程永光), Xiang-Hong Ge(葛向红), Bao-He Yuan(袁保合), Juan Guo(郭娟), Qian Sun(孙强), Er-Jun Liang(梁二军)
Chin. Phys. B . 2017, 26(10): 106501. **doi:** 10.1088/1674-1056/26/10/106501

Effect of ballistic electrons on ultrafast thermomechanical responses of a thin metal film

Qi-lin Xiong(熊启林), Xin Tian(田昕)
Chin. Phys. B . 2017, 26(9): 096501. **doi:** 10.1088/1674-1056/26/9/096501

Near-zero thermal expansion of $In_{2(1-x)}(HfMg)_xMo_3O_{12}$ with tailored phase transition

Yong-Guang Cheng(程永光), Yan-Chao Mao(毛彦超), Xain-Sheng Liu(刘献省), Bao-He Yuan(袁保合), Ming-Ju Chao(晁明举), Er-Jun Liang(梁二军)
Chin. Phys. B . 2016, 25(8): 086501. **doi:** 10.1088/1674-1056/25/8/086501

Phase transition and thermal expansion property of $Cr_{2-x}Zr_{0.5x}Mg_{0.5x}Mo_3O_{12}$ solid solution

Song Wen-Bo, Wang Jun-Qiao, Li Zhi-Yuan, Liu Xian-Sheng, Yuan Bao-He, Liang Er-Jun
Chin. Phys. B . 2014, 23(6): 066501. **doi:** 10.1088/1674-1056/23/6/066501

The phase transition, hygroscopicity, and thermal expansion properties of $Yb_{2-x}Al_xMo_3O_{12}$

Li Qiu-Jie,Yuan Bao-He,Song Wen-Bo,Liang Er-Jun,Yuan Bin
Chin. Phys. B . 2012, 21(4): 046501. **doi:** 10.1088/1674-1056/21/4/046501

Phase transition and near-zero thermal expansion of $Zr_{0.5}Hf_{0.5}VPO_7$*

Jun-Ping Wang(王俊平)[1,2], Qing-Dong Chen(陈庆东)[2], Sai-Lei Li(李赛磊)[3], Yan-Jun Ji(纪延俊)[1,2], Wen-Ying Mu(穆文英)[2], Wei-Wei Feng(冯伟伟)[2], Gao-Jie Zeng(曾高杰)[3], You-Wen Liu(刘友文)[1,†], and Er-Jun Liang(梁二军)[3,‡]

[1] *College of Science, Nanjing University of Aeronautics and Astronautics, Nanjing* 210016, *China*

[2] *College of Aeronautics and Engineering, Binzhou College, Binzhou* 256603, *China*

[3] *Key Laboratory of Materials Physics of Ministry of Education, School of Physical Science and Engineering, Zhengzhou University, Zhengzhou* 450052, *China*

(Received 9 March 2018; revised manuscript received 22 March 2018; published online 10 May 2018)

The $Zr_{0.5}Hf_{0.5}VPO_7$ is successfully synthesized by the solid-state method with near-zero thermal expansion. Powder x-ray diffraction (XRD), Raman spectroscopy, thermal dilatometry, and scanning electron microscopy (SEM) are used to investigate the structure, the phase transition, and the coefficient of thermal expansion (CTE) of $Zr_{0.5}Hf_{0.5}VPO_7$. The investigation results show that the samples are of the single cubic type with a space group of $Pa\bar{3}$ at room temperature (RT). It can be inferred that the superstructure is transformed from the $3\times3\times3$ superstructure to the $1\times1\times1$ ideal crystal in a temperature range between 310 K and 323 K. The CTE is measured by a dilatometer to be 0.59×10^{-6} K^{-1} (310 K–673 K). The values of intrinsic (XRD) and extrinsic (dilatometric) thermal expansion are both near zero. The results show that $Zr_{0.5}Hf_{0.5}VPO_7$ has near-zero thermal expansion behavior over a wide temperature range.

Keywords: near-zero thermal expansion, phase transition, x-ray diffraction (XRD), Raman spectrum

PACS: 65.40.De, 81.05.Je, 61.50.–f, 78.30.–j **DOI:** 10.1088/1674-1056/27/6/066501

1. Introduction

Negative thermal expansion (NTE) materials have the characteristics of heat shrinkage and cold rise, which can effectively control the expansion coefficient of material. The NTE material means it is possible to prepare composite materials each with an arbitrary expansion coefficient. The stress caused by thermal expansion and contraction is often the main cause of fatigue, performance decline, failures, and even breaking and falling off of the device. The NTE materials have extensive applications in many fields, such as optics, electronics, optical fiber communications, medicine, daily life, and many other fields. The NTE materials provide an effective way to control the thermal expansion coefficient and temperature range.[1–9] A series of NTE materials such as AM_2O_8 ($A=$ Zr, Hf; $M=$ W, Mo),[1–6] AM_2O_7 ($A=$ Zr, Hf; $M=$ V, P),[7–12] and $A_2M_3O_{12}$ ($A=$ Y, Sc, Fe; $M=$ W, Mo) has been reported.[13–19] Recently researchers investigated the materials with near-ZTE, which include $Mn_3Cu_{0.5}A_{0.5}N$ ($A=$ Ni, Sn)/Cu composites,[3] $Mn_3Ga_{0.5}Ge_{0.5}N$,[4] ZrW_2O_8/A ($A=ZrO_2$, Al_2O_3, etc.) composites,[5–7] $Zn_4B_6O_{13}$,[20] $ZrFeMo_2VO_{12}$,[21] and $HfMgMo_3O_{12}$.[22] The materials of MV_2O_7 ($M=$ Zr, Hf) have been extensively explored to reduce the phase transition temperature.[1,7] The AM_2O_7 family within the cubic $Pa\bar{3}$ space group possesses the coefficient of thermal expansion (CTE) varying linearly from low positive to large negative values. The ZrV_2O_7 is one of the most attractive NTE materials because of its stable structure and isotropic property. However, ZrV_2O_7 shows a two phase transition between 350 K and 375 K. In order to further control the expansion coefficient and the phase transition temperature of ZrV_2O_7, researchers considered the partial substitution of V by other cations. Hisashig *et al.* substituted Hf^{4+} instead of Zr^{4+} solid solution of $Zr_{1-x}Hf_xV_2O_7$. However, the phase transition point cannot be reduced effectively.[17] Yuan *et al.*[10] used Cu^{2+}/P^{5+} or Fe^{3+}/Mo^{5+} to replace Zr^{4+}/V^{5+}, but they found it was difficult to achieve a high solubility of the dopant. Many efforts have been made to design the composite materials with zero coefficient thermal expansion in a wide range of temperature. We have investigated the effects of substituting Hf^{4+}/P^{5+} instead of Zr^{4+}/V^{5+} and studied the effects of the phase transition and thermal expansion of ZrV_2O_7.

In this paper, a near-zero thermal expansion material of $Zr_{0.5}Hf_{0.5}VPO_7$ is synthesized by the solid state reaction method. Thermal dilatometry, XRD, and Raman spectra are used to investigate the CTE, anisotropy, and phase transition of $Zr_{0.5}Hf_{0.5}VPO_7$. It is found that the materials have the stable near-zero thermal expansion in a wide temperature range.

*Project supported by the National Natural Science Foundation of China (Grant Nos. 11574276, U173112, and 41401384), the Project of Shandong Provincial Higher Educational Science and Technology Program, China (Grant No. J17KB127), the Science and Technology Development Plans of Binzhou City, China (Grant Nos. 2014ZC0307 and 2015ZC0210), and Binzhou University Research Fund Project, China (Grant Nos. BZXYG1513 and BZXYG1706).

†Corresponding author. E-mail: ywliu@nuaa.edu.cn

‡Corresponding author. E-mail: ejliang@zzu.edu.cn

© 2018 Chinese Physical Society and IOP Publishing Ltd

2. Experimental procedure

$Zr_{0.5}Hf_{0.5}VPO_7$ samples were synthesized by the solid-state reaction method. The stoichiometric quantities of commercial chemicals of ZrO_2 (99%), HfO_2 (99%), $(NH_4)H_2PO_4$ (99%), and V_2O_5 (99%) were ground together thoroughly with an agate mortar for 2 h. The mixed powder was heated from room temperature (RT) to 1023 K in a furnace at a rate of 5 K/min, maintained at 1023 K for 5 h, and cooled down slowly in the furnace. The sintered powder was reground, pressed into pellets with a thickness of about 10 mm and a diameter of 10 mm, and then sintered again at 1023 K for 5 h. These processes were repeated twice to implement the complete reaction. The obtained compact pellets were kept for measuring their linear CTEs.

The samples were analyzed by XRD with a PANalytical X'Pert PRO x-ray diffractometer to identify the crystalline phase. Variable-temperature x-ray powder data were collected on a Rigaku (Japan, SmartLab 3 KW) diffractometer with Cu Kα ($\lambda = 0.15405$ nm) radiation. Unit cell dimensions above the phase transition temperature were determined with software of Powder X. The relative length changes at low temperature were measured with a LINSEIS DIL L75 dilatometer at heating and cooling rates of 5 K/min. The Raman spectra of the samples were tested by a LabRAM HR Evolution Raman spectrometer. The microstructures and energy dispersive spectra of the samples were examined with a scanning electron microscope (SEM, Model Quanta 250).

3. Results

3.1. Crystal structure analysis

Figure 1 shows the Raman spectra of the solid solutions of $Zr_{0.5}Hf_{0.5}VPO_7$. It is obvious that the Raman spectrum of $Zr_{0.5}Hf_{0.5}VPO_7$ is very different from those of ZrV_2O_7 and $Zr_{0.5}Hf_{0.5}$ V_2O_7, which is because the radius of a P^{5+} ion (38 pm) is smaller than that of a V^{5+} ion (59 pm). Previous studies have shown that the Raman modes in the ranges of 1100 cm^{-1}–910 cm^{-1}, 910 cm^{-1}–700 cm^{-1}, 550 cm^{-1}–450 cm^{-1}, and 400 cm^{-1}–300 cm^{-1} can be assigned to symmetric stretching (ν_1), asymmetric stretching (ν_3), asymmetric bending (ν_4), and symmetric bending (ν_2) modes of the VO_4 tetrahedron, respectively. The modes below 320 cm^{-1} originate from lattice modes, caused by Zr atom motion, translational and vibrational modes of VO_4, respectively.[1,9,23]

The most obvious change of the Raman spectrum of $Zr_{0.5}Hf_{0.5}VPO_7$ is the splitting of the symmetric stretching and asymmetric stretching modes of VO_4 tetrahedron around 1101 cm^{-1}–700 cm^{-1} in which there are strong peaks at 1101, 1061, and 972 cm^{-1} belonging to the symmetric stretching vibrations (ν_1 modes) of VO_4. The peaks at 887, 806, and 700 cm^{-1} belong to asymmetric stretching (ν_3 modes) of the VO_4. The peaks at 524 cm^{-1} and 474 cm^{-1} are ascribed to asymmetric bending (ν_4 modes). While those peaks at 403, 367, 344, 330, and 301 cm^{-1} originate from symmetric bending (ν_2) of the VO_4. The peaks at 282, 99, and 55 cm^{-1} originate from lattice modes, which arise from Zr atom motion, translational and librational modes of VO_4.[19]

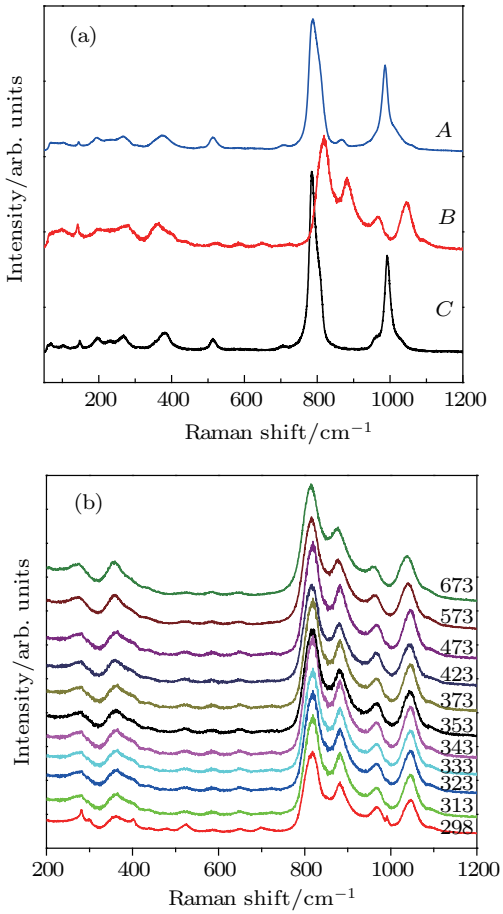


Fig. 1. (color online) (a) Raman spectra of (curve *A*) ZrV_2O_7, (curve *B*) $Zr_{0.5}Hf_{0.5}VPO_7$, and (curve *C*) $Zr_{0.5}Hf_{0.5}$ V_2O_7. (b) Temperature-dependent Raman spectra of $Zr_{0.5}Hf_{0.5}VPO_7$.

Figure 1(b) shows the temperature-dependent Raman spectra of $Zr_{0.5}Hf_{0.5}VPO_7$ in a temperature range from 298 K to 673 K. The modes at about 252, 302, 402, and 700 cm^{-1} become weakened with temperature increasing. An obvious protrusion appears near 280 cm^{-1} and becomes broadened as the temperature rises. The Raman peaks do not shift and they do not change their magnitudes, either, which suggests that $Zr_{0.5}Hf_{0.5}VPO_7$ keeps the cubic structure in a temperature range from 298 K to 673 K without phase transition. The results strongly suggest that $Zr_{0.5}Hf_{0.5}VPO_7$ is of a cubic structure and is transformed into the $1 \times 1 \times 1$ ideal crystal structure at RT.

Figure 2 shows the XRD patterns of the solid solutions of $Zr_{0.5}Hf_{0.5}VPO_7$, $Zr_{0.5}Hf_{0.5}V_2O_7$, and ZrV_2O_7 at RT. The diffraction peaks of $Zr_{0.5}Hf_{0.5}VO_7$ and $Zr_{0.5}Hf_{0.5}V_2O_7$ are

corresponding to the primary diffraction peaks of ZrV_2O_7 (ICDD-JCPDS-PDFNo. 01-088-0587), which crystallizes into the cubic structure with space group $Pa\bar{3}$. The diffraction peaks corresponding to the cubic structure recognized for ZrV_2O_7 were observed in $Zr_{0.5}Hf_{0.5}V_2O_7$.[11] However, those diffraction peaks for the superstructure almost disappear and the secondary peaks in a range of 33°–55° disappear in $Zr_{0.5}Hf_{0.5}VPO_7$. All results show that the $3 \times 3 \times 3$ superstructure of $Zr_{0.5}Hf_{0.5}VPO_7$ has disappeared. However, $Zr_{0.5}Hf_{0.5}V_2O_7$ has such diffraction peaks for the superstructure. These results further prove that P substitution is found to be more effective to suppress the superstructure of ZrV_2O_7.

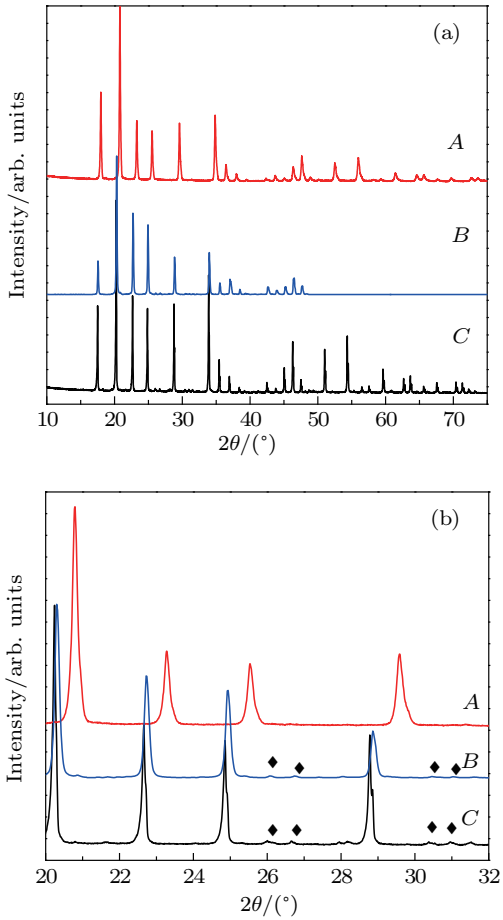


Fig. 2. (color online) (a) XRD patterns of (curve *A*) $Zr_{0.5}Hf_{0.5}VPO_7$, (curve *B*) $Zr_{0.5}Hf_{0.5}$ V_2O_7, (curve *C*) ZrV_2O_7. (b) Magnified part of patterns in panel (a) (symbol ♦ indicates the diffraction peaks of superstructures).

In order to confirm the crystal structure, the diffraction data are analyzed by the Rietveld and Le Bail methods in FullProf. The XRD data are refined in $Pa\bar{3}$ with the cubic structure of ZrV_2O_7 as a starting model. Figure 3 and Table 1 show the Rietveld analysis results of $Zr_{0.5}Hf_{0.5}VPO_7$. It is shown that the $Zr_{0.5}Hf_{0.5}VPO_7$ has a cubic structure with the space group $Pa\bar{3}$ ($R_p = 16.7$, $R_{wp} = 16.3$, $R_{exp} = 5.09$, $x^2 = R_{wp}/R_{exp} = 3.2$). The cell parameters are calculated to be $a = b = c = 8.5132$ Å and $\alpha = \beta = \gamma = 90°$ at RT. The refined results further indicate that $Zr_{0.5}Hf_{0.5}VPO_7$ adopts a cubic structure with the space group $Pa\bar{3}$ ($Z = 108$).

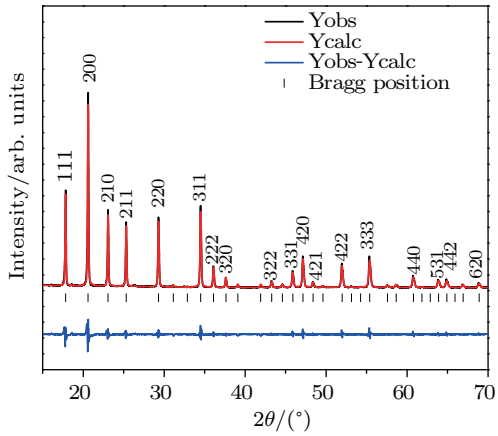


Fig. 3. (color online) Results of the Rietveld analysis of the XRD pattern for $Zr_{0.5}Hf_{0.5}VPO_7$ at room temperature ($R_p = 14.1$, $R_{wp} = 13.7$, $R_{exp} = 5.48$, $x^2 = R_{wp}/R_{exp} = 2.5$).

Table 1. Detailed XRD refinement results of $Zr_{0.5}Hf_{0.5}VPO_7$.

2θ/(°)	d/Å	Height	Area	FWHM
18.003	4.92336	9610.8	306261.7	0.32
20.819	4.26331	19172.1	632671.2	0.33
23.308	3.81332	6897.7	227585	0.33
25.568	3.48121	5905.8	194790.5	0.33
29.610	3.01456	6849.9	232887	0.34
34.871	2.57082	7843.6	258615.2	0.33
36.462	2.46223	2223.9	74046.1	0.34
38.021	2.36476	1223.2	39392.6	0.34
42.367	2.13168	680.8	22430.7	0.33
43.767	2.06671	989.6	31488.8	0.33
46.387	1.95588	2004.7	64659.9	0.33
47.665	1.90637	3322.2	112501.9	0.34
48.929	1.86003	798.8	25814.6	0.33
52.547	1.74018	2524.7	81599.2	0.33
55.998	1.64084	3166	101738.4	0.33
61.484	1.50693	1354.3	43929.8	0.35
64.624	1.44108	1119.9	36900.9	0.34
65.670	1.42063	1097.7	36683.9	0.35
69.680	1.34836	735.7	25548.1	0.36

3.2. Thermal expansion properties

The near-ZTE property of $Zr_{0.5}Hf_{0.5}VPO_7$ is investigated with a dilatometer. Figure 4 shows the variations of the relative length of $Zr_{0.5}Hf_{0.5}VPO_7$ and ZrV_2O_7 with temperatures. The $Zr_{0.5}Hf_{0.5}VPO_7$ presents an excellent stable zero thermal expansion property in the process of heating and cooling after undergoing a transition from superstructure to an ideal structure. The CET of $Zr_{0.5}Hf_{0.5}VPO_7$ is obtained to be 0.59×10^{-6} K^{-1} in a temperature from 310 K to 673 K. This result suggests that the $Zr_{0.5}Hf_{0.5}VPO_7$ has a better low thermal expansion property in a relatively low temperature range. It can also be obviously seen that there is no abrupt change below 310 K during the linear thermal expansion of the samples,

indicating that the $3 \times 3 \times 3$ superstructure has disappeared and no abrupt thermal expansion is observed, either.

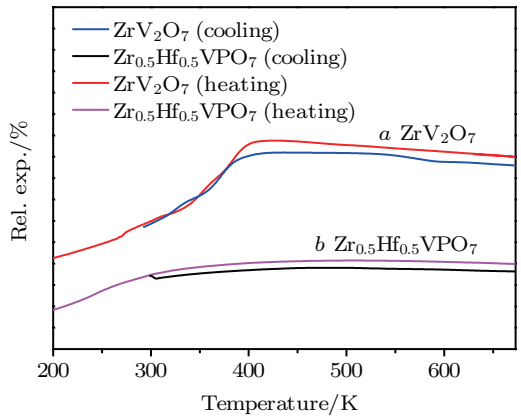


Fig. 4. (color online) Relative length changes of (curve *a*) ZrV_2O_7 and (curve *b*) $Zr_{0.5}Hf_{0.5}VPO_7$ with temperature increasing from 200 K to 673 K and temperature decreasing from 673 K to 310 K.

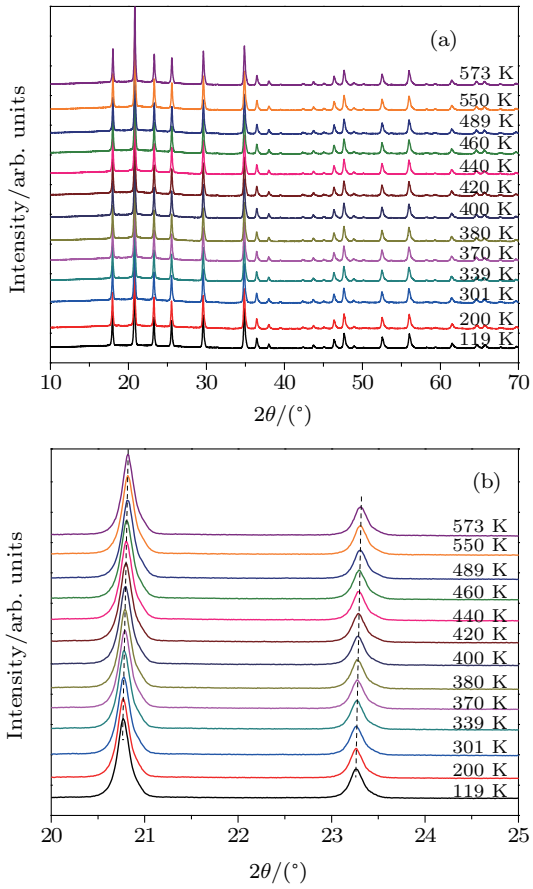


Fig. 5. (color online) (a) XRD patterns of $Zr_{0.5}Hf_{0.5}VPO_7$ at different temperatures. (b) Magnified part of patterns in panel (a).

Figure 5 shows the temperature dependent XRD patterns of $Zr_{0.5}Hf_{0.5}VPO_7$ in a temperature range from 119 K to 573 K. It is observed that the diffraction peaks of the XRD slightly shift to larger angles with temperature increasing (Fig. 5(b)). There are no obvious peaks appearing/disappearing in the XRD patterns in a temperature range from 119 K to 573 K. These results suggest that the samples keep cubic structures with temperature increasing. The cubic structures are found to be well consistent with space group $Pa\bar{3}$.

Figure 6 exhibits the variation of the cell volume with temperature, which is calculated by Powder X. It can be clearly seen that there is no abrupt thermal expansion above 400 K. That is because $Zr_{0.5}Hf_{0.5}VPO_7$ keeps a cubic structure in a temperature from 113 K to 673 K without phase transition. The CTE for volume is calculated to be $\alpha_{V2}^3 = 0.778 \times 10^{-6}$ K^{-1} in a temperature range of 400 K–573 K. This gives rise to a linear CTE$\alpha_{l2}^3 = 0.259 \times 10^{-6}$ K^{-1}, confirming that $Zr_{0.5}Hf_{0.5}VPO_7$ is intrinsically a ZTE material. This result is consistent with that from the Raman spectra, the $3 \times 3 \times 3$ superstructure remarkably disappears for $Zr_{0.5}Hf_{0.5}VPO_7$. The CTE for $Zr_{0.5}Hf_{0.5}VPO_7$ is measured to be 0.59×10^{-6} K^{-1} in a temperature range of 364 K–673 K by dilatometry. The difference between CTEs measured by the dilatometer and XRD can relate to the microstructure effect which can add a small negative component to the intrinsic linear expansion coefficient.

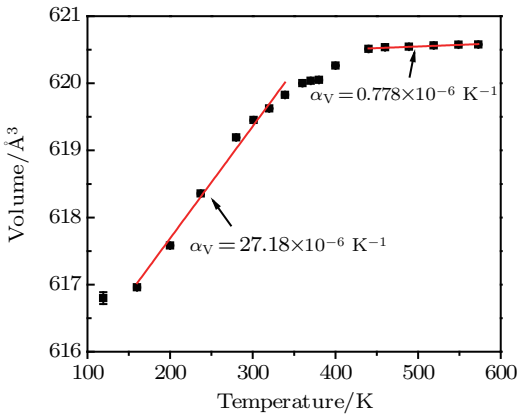


Fig. 6. (color online) Variation of the cell volume of $Zr_{0.5}Hf_{0.5}VPO_7$ with temperature.

The electronegativity of the cation and the M–O bond strength can be used to analyze the NTE of $Zr_{0.5}Hf_{0.5}VPO_7$. The electronegativity value of P^{5+} (2.19) is larger than that of V^{5+} (1.63). The bridging oxygen connected with V^{5+} or P^{5+} gains less negative charges with the content of P^{5+} increasing, which reduces the effective negative charge due to the oxygen-oxygen repulsion force and makes the transition harder from superstructure to ideal crystal structure. The partial substitution of V in ZrV_2O_7 by P reduces the symmetry and influences the transverse thermal vibration of V–O–V. The bond angle of V (P)–O–V in ZrV_2O_7 is close to 180° because the transverse motion of bridge O in V–O–V and P–O–V is responsible for the negative thermal expansion of ZrV_2O_7.[1,17]

Dilatometric results are slightly different from the results from the variable-temperature XRD and variable-temperature Raman spectra. The microstructure effects might be responsible for the cause of such a difference. Raman spectra and XRD reveal the internal molecular structure and vibration mode of

the unit cell. The Raman peak will change when the superstructure is disintegrated. The CTE from the dilatometer reflects the thermal expansion of bulk material, in which microcrack and poles are inevitable and may affect the measured results. The differences between intrinsic (XRD) and extrinsic (dilatometric) thermal expansion can be found in $Zr_{1-x}Fe_xV_{2-x}Mo_xO_7$,[7] $ZrFeMo_2VO_{12}$,[17] etc.

Figure 7 shows the SEM images of the sample. The microstructure of the grain morphology presents a spherical shape, which is closely arranged with the size of single short rod particle in a range from 2 μm to 6 μm. There are a few tiny gaps between rod particles. It should be noted that there are less pores in $Zr_{0.5}Hf_{0.5}VPO_7$ than in other samples even under the same sintering conditions.

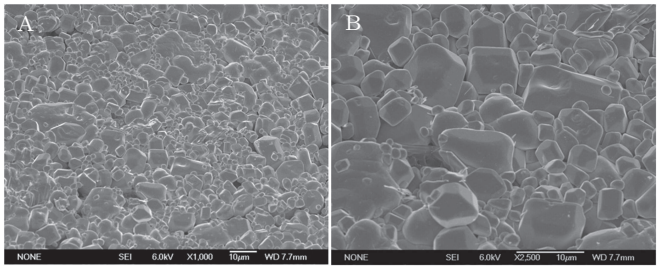


Fig. 7. SEM images of $Zr_{0.5}Hf_{0.5}VPO_7$ synthesized by solid state reaction.

4. Conclusions

A solid solution of $Zr_{0.5}Hf_{0.5}VPO_7$ with near-ZTE has successfully been synthesized by solid state reaction. Thermal dilatometry, XRD, and Raman spectra are used to investigate the compactness, the coefficient of thermal expansion, isotropy, and phase transition of $Zr_{0.5}Hf_{0.5}VPO_7$. The results show that stable near-zero thermal expansion of the prepared material goes over a wide temperature range. The CTE for $Zr_{0.5}Hf_{0.5}VPO_7$ is measured to be 0.59×10^{-6} K^{-1} in a temperature range of 310 K–673 K by dilatometry while it is calculated to be 0.259×10^{-6} K^{-1} (400 K–573 K) by XRD. The results from the dilatometer are slightly different from those from the variable-temperature XRD. The differences between the two methods are attributed to the effects of microstructure.

Acknowledgment

The author would like to thank Prof. Liang for his invaluable discussion and assistance.

References

[1] Yuan B H, Liu X S, Mao Y C, Wang J Q, Guo J, Cheng Y G, Song W B, Liang E J and Chao M J 2016 *Mater. Chem. Phys.* **170** 162
[2] Dai Y J, Huang R J, Wang W, Li L F and Sun Z H 2017 *Ceram. Int.* **43** 1608
[3] Ding L, Wang C, Na Y Y, Chu L H and Yan J 2011 *Scr. Mater.* **65** 687
[4] Yan J, Sun Y, Wang C, Chu L H, Shi Z X, Deng S H, Shi K W and Lu H Q 2014 *Scr. Mater.* **84–85** 19
[5] Yan X, Cheng X N, Yang X B and Zhang C H 2007 *Key Eng. Mater.* **353–358** 1235
[6] Yang X B, Cheng X N, Yan X H, Yang J, Fu T B and Qiu J 2007 *Compos. Sci. Technol.* **1167–1171** 67
[7] Yang X B, Xu J, Li H J, Cheng X N and Yan X H 2007 *J. Am. Ceram. Soc.* **90** 1953
[8] Romao C P, Perras F A, Wernerzwanziger U, Lussier J A and Miller K J 2015 *Chem. Mater.* **27** 2633
[9] Liang E J, Liang Y, Zhao Y, Liu J and Jiang Y J 2008 *J. Phys. Chem. A* **112** 12582
[10] Yuan B H, Liu X S, Mao Y C, Wang J Q, Guo J, Cheng Y G, Song W B, Liang E J and Chao M J 2016 *Mater. Chem. Phys.* **170** 162
[11] Yanase I, Kojima T and Kobayashi H 2011 *Solid State Commun.* **151** 595
[12] Mittal R and Chaplot S L 2008 *Phys. Rev. B* **78** 2599
[13] Yuan H L, Yuan B H, Li F and Liang E J 2012 *Acta Phys. Sin.* **61** 226502 (in Chinese)
[14] Song W B, Liang E J, Liu X S, Li Z Y, Yuan B H and Wang J Q 2013 *Chin. Phys. Lett.* **30** 126502
[15] Wu M M, Peng J, Zu Y, Liu Y D, Hu Z B, Liu Y T and Chen D F 2012 *Chin. Phys. B* **21** 116102
[16] Li Q J, Yuan B H, Song W B, Liang E J and Yuan B 2012 *Chin. Phys. B* **21** 046501
[17] Hisashige T, Yamaguchi T, Tsuji T and Yamamura Y 2006 *J. Ceram. Soc. Jpn.* **114** 607
[18] Evans J S O, Hanson J C and Sleight A W 1998 *Acta Crystallogr.* **54** 705
[19] Xiang H M, Feng Z H and Zhou Y C 2014 *J. Eur. Ceram. Soc.* **34** 1809
[20] Jiang X R, Molokeev M S, Gong P F, Yang Y, Wang W, Wang S H, *et al.* 2016 *Adv. Mater.* **28** 7936
[21] Chen D X, Yuan B H, Cheng Y G, Ge X H, Jia Y, Liang E J, *et al.* 2016 *Phys. Lett. A* **380** 4070
[22] Marinkovic B A, Jardim P M, Ari M, Avillez R R D, Rizzo F and Ferreira F F 2008 *Phys. Stat. Sol.* **245** 2514
[23] Hemamala U L C, El F, Muthu D V S, Krogh A M, Andersen, Carlson S, Ouyang L and Kruger M B 2007 *Solid State Commun.* **141** 680